Structural relaxation in a binary metallic melt: Molecular dynamics computer simulation of undercooled $Al_{80}Ni_{20}$

Subir K. Das,[1,2] Jürgen Horbach,[3] and Thomas Voigtmann[3,4]
[1]*Theoretical Sciences Unit, Jawaharlal Nehru Centre for Advanced Scientific Research, Jakkur, Bangalore 560064, India*
[2]*Institut für Physik, Johannes Gutenberg-Universität Mainz, Staudinger Weg 7, 55099 Mainz, Germany*
[3]*Institut für Materialphysik im Weltraum, Deutsches Zentrum für Luft- und Raumfahrt (DLR), 51170 Köln, Germany*
[4]*Fachbereich Physik, Universität Konstanz, 78457 Konstanz, Germany*
(Received 21 April 2008; revised manuscript received 29 July 2008; published 27 August 2008)

Molecular dynamics computer simulations are performed to study structure and structural relaxation in the glassforming metallic alloy $Al_{80}Ni_{20}$. The interactions between the particles are modeled by an effective potential of the embedded atom type. Our model of $Al_{80}Ni_{20}$ exhibits chemical short-range order (CSRO) that is reflected in a broad prepeak around a wave number of 1.8 $Å^{-1}$ in the partial static structure factor for the Ni-Ni correlations. The CSRO is due to the preference of Ni atoms to have Al rather than Ni atoms as nearest neighbors. By analyzing incoherent and coherent intermediate scattering functions as well as self-diffusion constants and shear viscosity, we discuss how the chemical ordering is reflected in the dynamics of the deeply undercooled melt. The q dependence of the α relaxation time as well as the Debye-Waller factor for the Al-Al correlations show oscillations at the location of the prepeak in the partial static structure factor for the Ni-Ni correlations. The latter feature of the Debye-Waller factor is well reproduced by a calculation in the framework of the mode coupling theory (MCT) of the glass transition, using the partial static structure factors from the simulation as input. We also check the validity of the Stokes-Einstein-Sutherland formula that relates the self-diffusion coefficients with the shear viscosity. We show that it breaks down already far above the mode coupling critical temperature T_c. The failure of the Stokes-Einstein-Sutherland relation is not related to the specific chemical ordering in $Al_{80}Ni_{20}$.

DOI: 10.1103/PhysRevB.78.064208 PACS number(s): 61.20.Lc, 61.20.Ja, 02.70.Ns, 64.70.pe

I. INTRODUCTION

The chemical ordering in binary metallic melts may lead to a structural arrangement of the atoms that is different from that of a closed-packed hard-sphere mixture, resulting in the occurrence of chemical short-range order (CSRO),[1–3] i.e., structural features on length scales that go beyond that of the typical distance between nearest-neighbor atoms. It is still an open question how mass transport and structural relaxation in metallic melts are affected by the presence of CSRO. In a recent study using a combination of quasielastic neutron scattering and molecular dynamics (MD) computer simulation,[4] this question was addressed for high-temperature Al-Ni melts at different compositions. It was shown that the CSRO indicates a nonadditive packing of Al and Ni atoms which is directly reflected in the diffusion dynamics. The essential structural features and the diffusion coefficients, as obtained by the simulation, were in good agreement with the neutron-scattering experiment. In this work, we extend the latter study to the consideration of a deeply undercooled $Al_{80}Ni_{20}$ melt, using MD simulation. The main aim is to elucidate the relation between chemical ordering and glassy dynamics for this system.

A theory that provides the link between the static structure and the relaxation dynamics in glassforming liquids is the mode coupling theory (MCT) of the glass transition.[5,6] In the framework of MCT, the dynamics is predicted from structural input, i.e., essentially from the partial static structure factors. The central dynamic quantities in MCT are time-dependent density correlation functions. For these quantities as well as for different transport coefficients, the theory makes a lot of detailed predictions that have stimulated many of the recent experiments on structural relaxation.[6,7] MD computer simulations have been very useful to test the predictions of MCT for different glassforming systems, in particular for a glassforming binary 80:20 Lennard-Jones (LJ) mixture studied extensively by Kob and co-workers.[8–14] More recently, analyses within the MCT framework have been successful for metallic alloys in particular.[15–22]

As we shall see below, the dynamics of $Al_{80}Ni_{20}$ is in many respects similar to that of the binary 80:20 Lennard-Jones mixture, in particular with respect to the validity of the MCT predictions. However, there are subtle differences between the two systems. Whereas the one-particle dynamics for Al and Ni is very similar in the considered Al-Ni mixture, the self-diffusion constants and one-particle relaxation times for A and B particles in the LJ system differ by up to a factor of 3 above the critical temperature of MCT, T_c. Moreover, the partial static structure factor for the Ni-Ni correlations, $S_{\mathrm{NiNi}}(q)$, exhibits a broad prepeak around a wave number of about 1.8 $Å^{-1}$, indicating an inhomogeneous distribution of Ni atoms on intermediate length scales. A similar feature is not seen in the LJ system. The prepeak in the Al-Ni mixture is reflected in the collective dynamics. Although the prepeak is only seen in the static structure factor for the Ni-Ni correlations, it can be identified in the dynamics for the Al-Al correlations, e.g., in the structural relaxation time $\tau_{\mathrm{AlAl}}(q)$. Below, we discuss all these peculiar features in regard to the chemical ordering in $Al_{80}Ni_{20}$.

Calculations in the framework of MCT are presented, based on the partial static structure factors from the MD simulation. We find that the Debye-Waller (DW) factors

$f^{(\alpha\alpha)}(q)$ are well reproduced by the theory, at least on a qualitative level. In particular, the occurrence of the Ni-Ni prepeak in the Al-Al dynamics is obtained by the MCT calculation. This demonstrates that MCT provides a basis toward the understanding of the subtle interplay between chemical ordering and structural relaxation in glassforming liquid mixtures.

A fundamental question, also addressed in the following, is about the relationship between one-particle transport and collective transport properties. In a recent publication,[23] we have investigated the relation between self-diffusion and interdiffusion, checking the validity of the so-called Darken equation[24] that expresses the interdiffusion constant D_{AB} by a simple linear combination of the self-diffusion constants. We found that the Darken equation is a good approximation for $Al_{80}Ni_{20}$ (and also for other mixtures such as $Al_{50}Ni_{50}$, as shown in another publication[25]). In this paper, we consider the Stokes-Einstein-Sutherland (SES) relation between self-diffusion and shear viscosity.[26,27] Different experiments on metallic alloys[28–30] suggest that the SES relation may work well above the critical mode coupling temperature T_c whereas one sees a decoupling of self-diffusion and viscosity below T_c. However, for a Zr based massive metallic glassformer,[31] it was shown experimentally that the SES relation is also invalidated above T_c. Computer simulations of the aforementioned LJ mixture[32] and of hard-sphere-like colloidal glassformers[33] as well as of silica[34] again indicate that the SES relation fails already above T_c. Here, we consider the SES relation for a realistic model of $Al_{80}Ni_{20}$ and quantify the decoupling of self-diffusion and shear viscosity in this system.

The rest of the paper is organized as follows: In Sec. II, we present the model and discuss details of the simulation technique as well as of the MCT calculations. The results for the static structure and structural relaxation are presented in Sec. III. Section IV concludes this paper with a brief summary and discussion of our results and future scopes.

II. TECHNICAL DETAILS

A. Model and details of the simulation

In order to model the interaction between the atoms in $Al_{80}Ni_{20}$, we use a potential of the embedded atom type (EAM) that has been recently proposed by Mishin *et al.*[35] This model potential has been proven successful to describe rather accurately various structural and dynamic properties of Al-Ni melts[4,23] as well as the crystallization kinetics from the melt for B2-$Al_{50}Ni_{50}$.[25]

In the framework of an EAM potential, the total potential energy of a binary system such as $Al_{80}Ni_{20}$ reads

$$V = \frac{1}{2}\sum_{ij} u_{\alpha_i\alpha_j}(r_{ij}) + \sum_i F_{\alpha_i}(\bar{\rho}_i), \tag{1}$$

with $u_{\alpha_i\alpha_j}(r_{ij})$ as the pair interaction potential between particles i and j of the ionic species α_i and α_j, respectively, separated by a distance $r_{ij}=|\mathbf{r}_i-\mathbf{r}_j|$, and F_{α_i} as the embedding energy of species α_i at site i due to the electron density $\bar{\rho}_i$ from all other atoms. Here, $\bar{\rho}_i$ can be written as

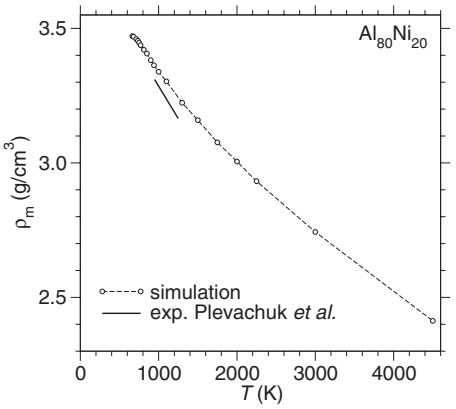

FIG. 1. Plot of the total mass density vs temperature at zero pressure, $p=0$. The dashed line is a guide to the eye. The solid bold line represents experimental data by Plevachuk *et al.* (Ref. 38).

$$\bar{\rho}_i = \sum_{j\neq i} \rho_{\alpha_j}(r_{ij}), \tag{2}$$

with $\rho_{\alpha_j}(r_{ij})$ as the electron density at i due to the ionic species α_j at a distance r_{ij}. For the sake of brevity we do not write down the exact functional forms of $u_{\alpha\beta}$ $(\alpha,\beta=\mathrm{Al,Ni})$ as well as the embedding energies and electron densities, but refer to Ref. 35 for details.

The simulations were performed at zero external pressure $(p=0)$, in order to allow for a direct comparison to experiments under ambient pressure. Systems of $N=1500$ particles $(N_{Al}=1200$ and $N_{Ni}=300)$ are put in a cubic simulation box with periodic boundary conditions. First, Monte Carlo (MC) simulations in the NpT ensemble[36] (with $p=0$) were performed at each temperature, using a combination of standard particle displacement moves and allowing the volume to fluctuate. In the particle displacement moves, trial displacements were randomly chosen from the interval $[-\sigma/50, \sigma/50]$, where σ is the average interatomic separation. At the end of N trial displacements, an isotropic volume move of random magnitude ΔV between $[-V/100, V/100]$ was tried. In the volume moves the new particle positions were rescaled with an appropriate factor according to the volume change. These moves were accepted or rejected according to a Metropolis criterion (for details see Ref. 36). Depending upon the temperature, the length of the MC simulations extended between 10^5 to 2×10^6 cycles, where a MC cycle consists of N displacement moves and a single volume move.

The average volume was obtained from the asymptotic flat portion of the curve extending over a reasonable length. In Fig. 1, we present the total mass density of particles, ρ_m, as a function of temperature, as obtained from the zero pressure MC simulations. Although the density changes significantly from about 2.5 g/cm^3 around 4000 K to about 3.5 g/cm^3 around 650 K, we shall see below that the relaxation dynamics in this temperature range is qualitatively similar to that found in constant volume simulations of a binary Lennard-Jones mixture.[7–10] Also shown in Fig. 1 are experimental data around the liquidus temperature $T_L=1263$ K (Ref. 37) that were obtained by Plevachuk *et al.*[38] using electromagnetic levitation techniques. We find that the

MD simulation agrees with experimental data within a 2%–3% margin.

At each temperature, the average volume, as obtained from the MC runs, was used as an input to the MD simulations. In the latter simulations, Newton's equations of motion were integrated with the velocity form of the Verlet algorithm,[36,39] using a time step of 1 fs for $T \geq 1500$ K and 2.5 fs for lower temperatures. The masses of Al and Ni atoms were set to $m_{\mathrm{Al}}=26.981539$ amu and $m_{\mathrm{Ni}}=58.693$ amu.

First, the system was fully equilibrated at high temperatures ($T \geq 2260$ K), by performing runs over 10^5 time steps in the *NVT* ensemble. In order to keep the temperature constant, we applied the Andersen thermostat where after every 50 cycles we have chosen new velocities from a Maxwell-Boltzmann distribution in accordance with the temperature of the system.[39] Appropriate care was taken to equilibrate the system at each new temperature: Before starting the production runs at each lower temperature, an *a priori* estimate of the equilibration time t_{equ} was made by reasonable extrapolation of the relaxation time from higher temperature and in addition to the MC runs (as described above), a further thermalization was done in the *NVT* ensemble for times larger than t_{equ} in the MD simulations. Finally these equilibrated configurations were used as initial configurations for the production runs of MD simulations in the microcanonical ensemble. The temperatures considered were 4490, 2994, 2260, 1996, 1750, 1496, 1300, 1100, 998, 940, 893, 847, 810, 777, 754, 735, 715, 700, 680, and 665 K. At the lowest temperature $T=665$ K, both the length of the equilibration and the production runs extended over 40×10^6 time steps, corresponding to 100 ns real time. To improve the statistics, eight runs over independent initial configurations were performed at each temperature.

For the calculation of the shear viscosity η, additional production runs were done in the temperature range $4490\ \mathrm{K} \geq T \geq 715$ K that extended the aforementioned production runs by a factor of 10. This was necessary in order to obtain a reasonable statistics for η. Note that the same runs were also used to determine the interdiffusion constant D_{AB}. A detailed study of the temperature dependence of D_{AB} can be found elsewhere.[23]

Let us point out that all simulation results presented in the following are obtained from runs that were fully equilibrated before any static or time-dependent averages were calculated.

B. MCT calculations

MCT predicts drastic changes in the dynamics of glass-forming liquids arising from relatively minor changes in the average equilibrium structure. In its most common form, MCT requires the input of partial static structure factors $S_{\alpha\beta}(q)$ to take the information about the liquid structure. The functions $S_{\alpha\beta}(q)$ are defined by[40]

$$S_{\alpha\beta}(q) = \frac{1}{N}\sum_{k_\alpha=1}^{N_\alpha}\sum_{l_\beta=1}^{N_\beta}\langle \exp\{i\mathbf{q}\cdot[\mathbf{r}_{k_\alpha}-\mathbf{r}_{l_\beta}]\}\rangle, \tag{3}$$

where the indices k_α, l_β correspond to particles of species α and β, respectively ($\alpha,\beta=\mathrm{Al},\mathrm{Ni}$). Due to the isotropy of the considered systems, the structure factors [Eq. (3)] depend on wave-vector $\mathbf{q}$ only through the magnitude $q=|\mathbf{q}|$.

For all but the simplest model potentials, the functions $S_{\alpha\beta}(q)$ have to be determined from computer simulation, or from scattering experiments, although disentangling the partial contributions in mixtures can be challenging for the latter. A recent MCT study of a Zr-Ni mixture[22] used the $S_{\alpha\beta}(q)$ from a set of neutron-scattering studies, that were, however, restricted to a single temperature. In our study, we base MCT calculations for $\mathrm{Al_{80}Ni_{20}}$ on the $S_{\alpha\beta}(q)$ obtained from the MD simulation at the temperatures $T=2000$ K, 1500 K, and 1000 K, with linear interpolation between those points.

The solution to the MCT equations of motion is the matrix of partial dynamic structure factors $\mathbf{S}(q,t)$. Its elements, $S_{\alpha\beta}(q,t)$, are a straightforward generalization of the partial static structure factors:[7]

$$S_{\alpha\beta}(q,t) = \frac{1}{N}\sum_{k_\alpha=1}^{N_\alpha}\sum_{l_\beta=1}^{N_\beta}\langle \exp\{i\mathbf{q}\cdot[\mathbf{r}_{k_\alpha}(t)-\mathbf{r}_{l_\beta}(0)]\}\rangle. \tag{4}$$

At $t=0$, the functions $S_{\alpha\beta}(q,t)$ yield the partial static structure factors, i.e., $\mathbf{S}(q,t=0)\equiv\mathbf{S}(q)$. For the diagonal elements of these matrices, $\alpha=\beta$, it is convenient to consider normalized quantities, the so-called coherent intermediate scattering functions,[7] defined by

$$F^{(\alpha\alpha)}(q,t) = S_{\alpha\alpha}(q,t)/S_{\alpha\alpha}(q). \tag{5}$$

A similar definition for the unequal correlations, $\alpha\neq\beta$, is not sensible, since the static structure factor $S_{\alpha\beta}(q)$ for $\alpha\neq\beta$ has zero-crossings (see Fig. 4). The one-particle dynamics is quantified by the self-part of the intermediate scattering function,

$$F_s^{(\alpha)}(q,t) = \frac{1}{N_\alpha}\sum_{j=1}^{N_\alpha}\langle \exp\{i\mathbf{q}\cdot[\mathbf{r}_j(t)-\mathbf{r}_j(0)]\}\rangle. \tag{6}$$

This function is also called incoherent intermediate scattering function.

The MCT equations of motion were solved numerically as outlined in Ref. 41. These equations are given by

$$\mathbf{J}^{-1}(q)\partial_t^2\mathbf{S}(q,t) + \mathbf{S}^{-1}(q)\mathbf{S}(q,t) + \int_0^t \mathbf{M}(q,t-t')\partial_{t'}\mathbf{S}(q,t')dt' = \mathbf{0}, \tag{7}$$

where $J_{\alpha\beta}(q)=q^2k_BT/m_\alpha\delta_{\alpha\beta}$ sets the thermal velocities for the short-time dynamics. $\mathbf{M}(q,t)$ is the memory function matrix of generalized fluctuating forces, which in the MCT approximation is written as

$$M_{\alpha\beta}(q,t) = \frac{1}{2q^2}\frac{n}{c_\alpha c_\beta}\int\frac{d^3k}{(2\pi)^3} \times \sum_{\alpha'\beta'\alpha''\beta''} V_{\alpha\alpha'\alpha''}(\vec{q},\vec{k})V_{\beta\beta'\beta''}(\vec{q},\vec{k}) \times S_{\alpha'\beta'}(k,t)S_{\alpha''\beta''}(p,t) \tag{8}$$

with $p=|\vec{q}-\vec{k}|$. Here, n is the number density, and c_α are the number concentrations, $c_{\mathrm{Al}}=0.8$ and $c_{\mathrm{Ni}}=0.2$ in our case. The

vertices $V_{\alpha\alpha'\alpha''}(\vec{q},\vec{k})=(\vec{q}\vec{k}/q)c_{\alpha\alpha'}(k)\delta_{\alpha\alpha''}+(\vec{q}\vec{p}/q)c_{\alpha\alpha''}(p)\delta_{\alpha\alpha'}+qnc_\alpha c^{(3)}_{\alpha\alpha'\alpha''}(\vec{q},\vec{k})$ contain only equilibrium static correlations, viz. the matrix of direct correlation functions $\mathbf{c}(q)$ defined by $\mathbf{S}(q)$ through the Ornstein-Zernike relation.[40] $c^{(3)}$ denotes the corresponding static triplet correlation function,[42] which we set to zero in the following. The latter approximation has been justified in a study of the binary Lennard-Jones mixture[43] (mentioned in the Introduction) where it was shown that the triplet correlation functions do not give noticeable contributions to the vertices $V_{\alpha\alpha'\alpha''}$. We assume a similar conclusion to hold in dense metallic melts such as our Al-Ni mixture.

MCT describes the slowing down of the dynamics, connected to an increase in relaxation times for the $\mathbf{S}(q,t)$, as the coupling described by the $V_{\alpha\alpha'\alpha''}$ increases smoothly through a variation of control parameters such as the temperature T. The divergence of relaxation times defines the MCT critical point T_c. No such divergence is observed in experiment or simulation, but the scaling laws connected to T_c describing the asymptotic shape of the correlation functions and a power-law variation in relaxation times have been seen in experiments of various systems.[6] Hence, the MCT critical point provides a useful, well-defined concept to discuss the slow dynamics of glassforming systems.

Equation (8) indicates that the memory kernel is a symmetric bilinear form of the density correlators, $\mathbf{M}(q,t)=\mathcal{F}[\mathbf{S}(t),\mathbf{S}(t)](q)$. At $t\to\infty$, the bifurcation, occurring at T_c, can be identified by the long-time limit $\mathbf{F}(q)=\lim_{t\to\infty}\mathbf{S}(q,t)$. The $F_{\alpha\beta}(q)$ are called the glass form factors (or Debye-Waller factors) and are solutions of the equation

$$\mathbf{F}(q)=\mathbf{S}(q)-\{(\mathbf{S}(q))^{-1}+\mathcal{F}[\mathbf{F},\mathbf{F}](q)\}^{-1}. \tag{9}$$

From this equation, $\mathbf{F}(q)$ can be calculated by an iteration scheme. For sufficiently small vertices, the liquid solution $\mathbf{F}(q)=\mathbf{0}$ is obtained, while in the glass the solution $\mathbf{F}(q)\neq\mathbf{0}$ is found. Below, we present MCT results for the normalized DW factors $f^{(\alpha\alpha)}(q)=F^{(\alpha\alpha)}(q)/S_{\alpha\alpha}(q)$, as well as for $f_s^{(\alpha)}(q)=F_s^{(\alpha)}(q)/S_{\alpha\alpha}(q)$, the so-called Lamb-Mößbauer (LM) factors, and compare them with the results from the MD simulation.

III. RESULTS

In this section we present the results for structural and dynamic quantities of $Al_{80}Ni_{20}$ from the MD simulations. The discussion of the chemical ordering in terms of partial pair correlation functions and various structure factors is followed by an analysis of structural relaxation and mass transport properties.

A. Structure

A useful quantity to characterize the short-range order in a liquid as well as the chemical ordering in a liquid mixture is the pair correlation function. For a binary AB mixture, three partial pair correlation functions $g_{\alpha\beta}(r)$ $(\alpha,\beta=\mathrm{A},\mathrm{B})$ are defined as[7]

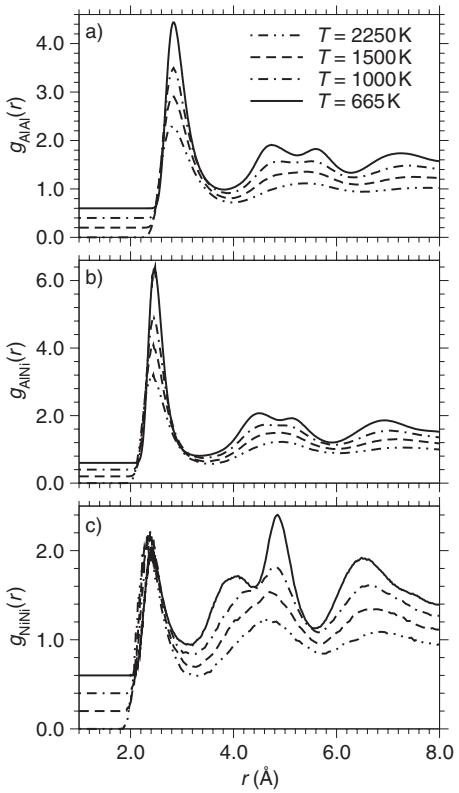

FIG. 2. Partial radial distribution function $g_{\alpha\beta}(r)$ $(\alpha,\beta=\mathrm{Al},\mathrm{Ni})$ for (a) AlAl, (b) AlNi, and (c) NiNi, at different temperatures, as indicated. For clarity of presentation, the curves at different temperatures are separated from each other in steps of 0.2.

$$g_{\alpha\beta}(r)=\frac{N}{\rho N_\alpha(N_\beta-\delta_{\alpha\beta})}\left\langle\sum_{i=1}^{N_\alpha}\sum_{j=1}^{N_\beta}{}'\,\delta(r-r_{ij})\right\rangle, \tag{10}$$

where the prime in the second sum means that $i\neq j$ if $\alpha=\beta$; $\delta_{\alpha\beta}$ is the Kronecker delta. Physically $g_{\alpha\beta}(r)$ is proportional to the conditional probability of finding a particle of species β at a distance r from a particle of species α fixed at the center. In case of an ideal gas, there are no correlations between the particles for all distances r. Then, the functions $g_{\alpha\beta}(r)$ are equal to one. For a liquid, the limit $g_{\alpha\beta}(r)\to 1$ is approached for $r\to\infty$.

In Fig. 2, we show functions $g_{\alpha\beta}(r)$ for the different correlations $\alpha\beta=\mathrm{AlAl},\mathrm{AlNi},\mathrm{NiNi}$ at various temperatures in the range 2250 K $\geq T\geq$ 665 K. For clarity of presentation, the curves are shifted from each other by a fixed distance on the ordinate. For the Al-Al correlations, there is an increase in the height of the first peak with decreasing temperature, located around 2.84 Å, and, at the lowest temperature, $T=665$ K, a splitting of the second peak into two peaks around 4.73 Å and 5.6 Å is seen, with a slightly larger amplitude of the peak at the smaller distance. The function $g_{\mathrm{AlNi}}(r)$ shows a similar behavior. Here, the first peak is located around 2.47 Å, i.e., at slightly smaller distance than in the Al-Al correlations. At $T=665$ K, the second peak in $g_{\mathrm{AlNi}}(r)$ splits into one around 4.5 Å and another one around 5.13 Å. A different behavior is seen for $g_{\mathrm{NiNi}}(r)$. In this case, the amplitude of the first peak around 2.42 Å decreases sig-

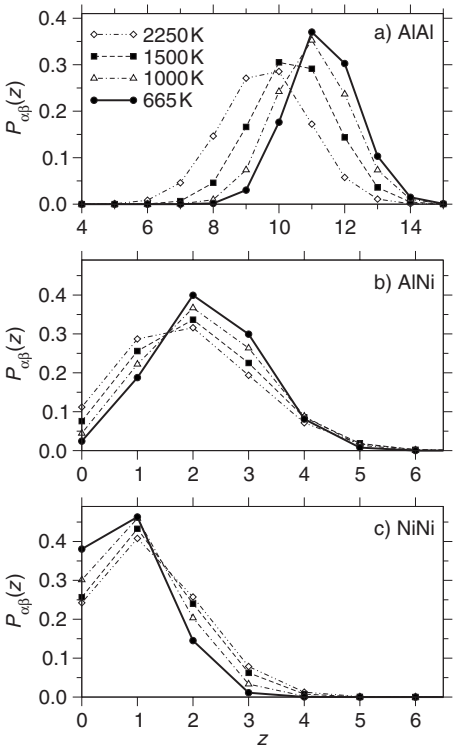

FIG. 3. Coordination number distributions $P_{\alpha\beta}(z)$ for (a) $\alpha\beta$ =AlAl, (b) $\alpha\beta$=AlNi, and (c) $\alpha\beta$=NiNi at different temperatures, as indicated.

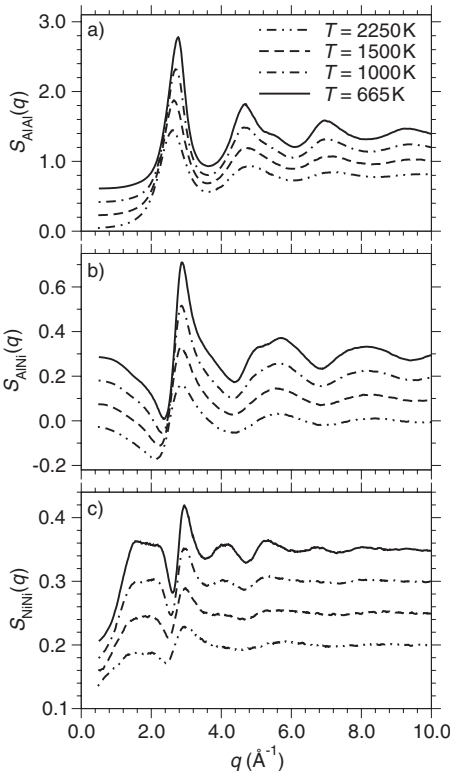

FIG. 4. Partial structure factors $S_{\alpha\beta}(q)$ (α,β=Al,Ni) for (a) AlAl, (b) AlNi, and (c) NiNi, at different temperatures, as indicated. The plots at different temperatures are separated from each other in steps of 0.2 in (a), 0.1 in (b), and 0.05 in (c).

nificantly with decreasing temperature and the splitting of the second peak (with peaks around 4.07 Å and around 4.85 Å) is highly asymmetric, yielding a significantly larger amplitude of the peak at the larger distance. This indicates that the effective repulsion between two neighboring Ni particles is larger than that between AlNi and AlAl pairs. Thus, Ni particles tend to stay further apart from each other at low temperatures, preferring Al atoms as nearest neighbors and this is possible since the Ni atoms are the minority species in $Al_{80}Ni_{20}$. This behavior is typical for a liquid mixture with a strong ordering behavior, i.e., there is no tendency toward a liquid-liquid demixing. Indeed, it is well known from the experimental phase diagram that Al-Ni does not exhibit a miscibility gap.[37]

Other quantities that characterize the chemical ordering in a liquid mixture are the coordination number distributions $P_{\alpha\beta}(z)$ ($\alpha\beta$=AlAl,AlNi,NiNi) that are shown in Fig. 3. The coordination number z, which corresponds to $P_{\alpha\beta}(z)$, is given by the number of particles of type β that are in the first-nearest-neighbor shell around a particle of type α. We define the radius of the first-nearest-neighbor shell via the first minima of the pair correlation functions $g_{\alpha\beta}(r)$. For the following analysis we used the values 3.8 Å, 3.35 Å, and 3.2 Å for the Al-Al, Al-Ni, and Ni-Ni correlations, respectively. As we can infer from $P_{\mathrm{AlAl}}(z)$, the number of Al neighbors around an Al atom increases up to an average value between 11 and 12 at low temperatures. The most likely values for the number of Ni neighbors around an Al atom are z=2 and z=3 at low temperature. The number of Ni neighbors around an Ni atom decreases with decreasing temperature, in agreement with the behavior observed for $g_{\mathrm{NiNi}}(r)$. At T=665 K, about 85% of the Ni atoms have either no or only one Ni neighbor. As we shall see in the following, the "avoidance" of Ni pairs is associated with the presence of CSRO on an intermediate length scale, i.e., on a length scale that goes beyond that of nearest-neighbor distances.

The radial distribution functions are essentially the inverse Fourier transforms of the partial static structure factors $S_{\alpha\beta}(q)$ defined in Eq. (3). In Fig. 4, the three partial structure factors are displayed for different temperatures. The first peak in $S_{\mathrm{AlAl}}(q)$ is due to the presence of repeating Al-Al nearest-neighbor units in the real-space structure. As typical for undercooled liquids, the second peak in $S_{\mathrm{AlAl}}(q)$ develops a shoulder at low temperature (for a discussion of this shoulder in various undercooled metallic melts, see Ref. 44). In $S_{\mathrm{AlNi}}(q)$, a peak with a negative amplitude, located slightly above 2.0 Å^{-1}, is seen. This feature is similar to what has been found for the 80:20 LJ mixture introduced by Kob and Andersen. Such negative amplitudes in the cross term of the partial static structure factors, expressing the avoidance of very long-ranged AB correlations, are already seen in hard-sphere mixtures, although there the dip before the main peak is less pronounced. A very peculiar feature is found in $S_{\mathrm{NiNi}}(q)$: A broad prepeak forms around 1.8 Å^{-1} that becomes more pronounced with decreasing temperature. This prepeak indicates the preference of Ni atoms in $Al_{80}Ni_{20}$ for having Al atoms as nearest neighbors and being well separated from other Ni atoms. Thus, the avoidance of neighbor-

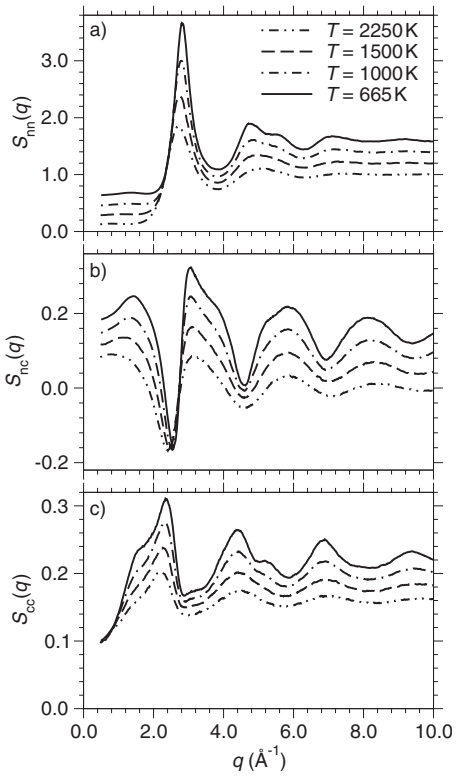

FIG. 5. Bhatia-Thornton structure factors $S_{nn}(q)$ (a), $S_{nc}(q)$ (b), and $S_{cc}(q)$ (c) at different temperatures, as indicated. The curves at different temperatures are separated from each other by 0.2 in (a), 0.04 in (b), and 0.02 in (c).

ing Ni pairs leads to structural order on intermediate length scales, indicated by a prepeak in $S_{\mathrm{NiNi}}(q)$. In a recent publication, we have described the structure, underlying the latter prepeak, as a stringlike arrangement of the Ni atoms.[4]

The specific chemical ordering of Ni atoms in $Al_{80}Ni_{20}$ can be most clearly seen in the Bhatia-Thornton structure factors.[45] In these functions, the correlations of number density and concentration fluctuations are considered. For a binary system, three independent Bhatia-Thornton structure factors exist, measuring the autocorrelations of number density $[S_{nn}(q)]$ and concentration density $[S_{cc}(q)]$ as well as the mixed correlations between number and concentration density $[S_{nc}(q)]$. The functions can be expressed by linear combinations of the partial static structure factors as

$$S_{nn}(q) = S_{\mathrm{AlAl}}(q) + 2S_{\mathrm{AlNi}}(q) + S_{\mathrm{NiNi}}(q), \tag{11}$$

$$S_{nc}(q) = c_{\mathrm{Ni}}S_{\mathrm{AlAl}}(q) - c_{\mathrm{Al}}S_{\mathrm{NiNi}}(q) + (c_{\mathrm{Ni}} - c_{\mathrm{Al}})S_{\mathrm{AlNi}}(q), \tag{12}$$

$$S_{cc}(q) = c_{\mathrm{Ni}}^2 S_{\mathrm{AlAl}}(q) + c_{\mathrm{Al}}^2 S_{\mathrm{NiNi}}(q) - 2c_{\mathrm{Al}}c_{\mathrm{Ni}}S_{\mathrm{AlNi}}(q), \tag{13}$$

where $c_{\mathrm{Al}}=N_{\mathrm{Al}}/N$ and $c_{\mathrm{Ni}}=N_{\mathrm{Ni}}/N$ are the total concentrations of Al and Ni atoms, respectively.

In Fig. 5, we present the Bhatia-Thornton structure factors at different temperatures. Again the curves have been shifted from each other for clarity of presentation. The function $S_{nn}(q)$ is very similar to $S_{\mathrm{AlAl}}(q)$; one can hardly identify the presence of the aforementioned prepeak in $S_{nn}(q)$. However, this prepeak, albeit with a different shape than in $S_{\mathrm{NiNi}}(q)$, is present in $S_{nc}(q)$ and, as a shoulder, also in $S_{cc}(q)$. The appearance of the prepeak in $S_{cc}(q)$ clearly indicates that this feature is due to the specific chemical ordering of Ni atoms in $Al_{80}Ni_{20}$.

B. Dynamics

In a highly viscous liquid, time-dependent density correlation functions as well as other correlation functions that have a coupling to density fluctuations reveal structural relaxation processes that show a time-scale separation from dynamic processes on microscopic scales (e.g., phonons). In an atomistic system such as $Al_{80}Ni_{20}$, the microscopic dynamics occurs on a subpicosecond time scale, whereas structural relaxation can extend to arbitrary time scales, depending on the considered temperature. A glass is formed if the typical relaxation time of a system exceeds the accessible time scale in an experiment or simulation. Note that, as mentioned above, we concern ourselves only with fully equilibrated simulation runs, i.e, states above the glass transition.

We start our discussion with an analysis of the one-particle dynamics. A simple quantity, which shows already all the features that characterize the relaxation dynamics of an undercooled melt, is the mean-squared displacement (MSD) of a tagged particle. It is defined as

$$\langle r_\alpha^2(t)\rangle = \langle[\mathbf{r}_{t,\alpha}(0) - \mathbf{r}_{t,\alpha}(t)]^2\rangle, \tag{14}$$

where $\mathbf{r}_{t,\alpha}(t)$ denotes the position of a tagged particle of type α (α=Al,Ni) at time t, and $\langle\ldots\rangle$ implies the average over independent runs as well as over particles of the same species.

In Fig. 6, we show $\langle r_\alpha^2(t)\rangle$ for Al and Ni particles for all simulated temperatures, on a log-log scale. The behavior is very similar to what has been observed in computer simulations of many other glassforming liquids: At very short times, a ballistic regime is seen ($\langle r_\alpha^2(t)\rangle \propto t^2$). Then, at high temperatures, a rapid crossover to the linear diffusive regime occurs, $\langle r_\alpha^2(t)\rangle = 6D_\alpha t$ (with D_α as the self-diffusion constant for a particle of species α). At low temperatures, a plateau is observed at intermediate times, where the MSD does not increase, but rather stays constant at about $\langle r_\alpha^2(t)\rangle \approx 0.2$ Å^2. This plateau indicates the onset of the "cage effect:" Each atom sits in a "cage" formed by its nearest neighbors and the lower the temperature the more time it takes until the atom can "escape from the cage."

As we can infer from Fig. 6, the mean-squared displacements for Al and Ni atoms are almost identical at a given temperature. This may be explained by the structural arrangement of Al and Ni atoms in $Al_{80}Ni_{20}$. As we have seen above, Ni atoms have a strong preference to avoid other Ni atoms as nearest neighbors. Therefore, Ni atoms are built into an Al environment and thus, the mean-squared displacements are very similar for Al and Ni atoms. This is also manifested in the self-diffusion constants D_α, as determined from the mean-squared displacements. The data for the self-diffusion constants are published elsewhere.[23] D_{Al} and D_{Ni}

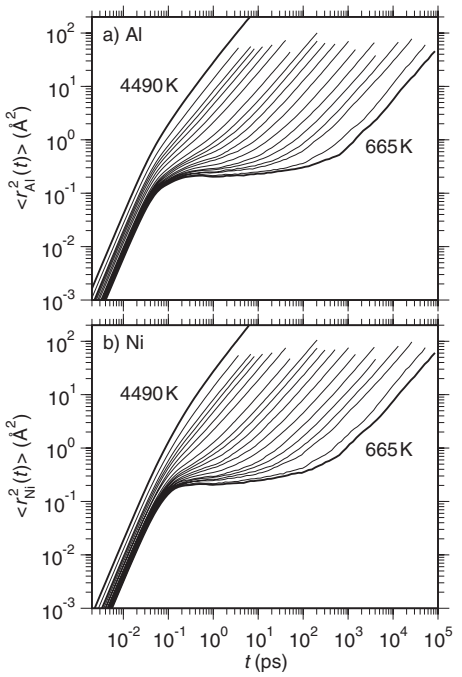

FIG. 6. Double-logarithmic plot of the mean-squared displacements $\langle r_\alpha^2(t)\rangle$ (α=Al,Ni) as a function of time t for (a) Al atoms and (b) Ni atoms. The results for all the simulated temperatures in the range 4490 K$\geq T\geq$665 K are shown.

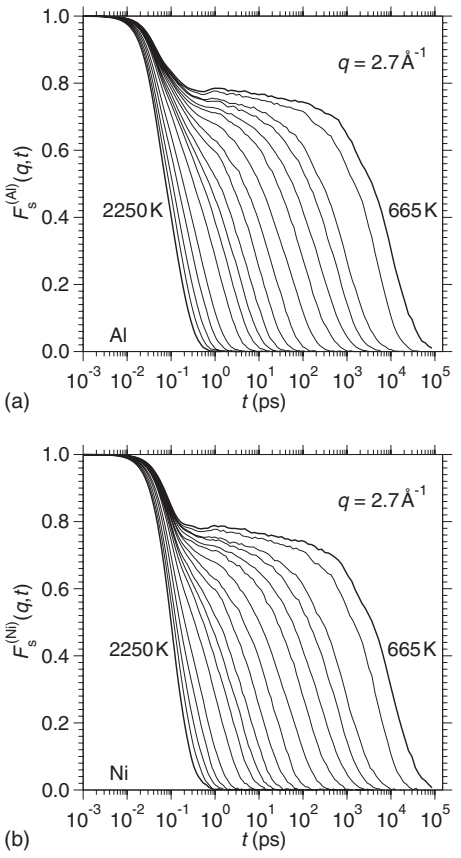

FIG. 7. Log-linear plot of the incoherent intermediate scattering functions $F_s^{(\alpha)}(q,t)$ (α=Al,Ni) for all the simulated temperatures for (a) Al and (b) Ni. The wave number is q=2.7 Å^{-1}. This wave number is close to the location of the first maximum in $S_{AlAl}(q)$.

are in fact almost identical over the whole temperature range 4490 K$\geq T\geq$665 K. The similarity between D_{Al} and D_{Ni} holds only for Al rich Al-Ni alloys. For Ni rich compositions, the Ni diffusion is significantly faster than the Al diffusion,[4] at least for the interaction model used in our simulations.

In contrast to our Al-Ni mixture, the 80:20 LJ mixture of Kob and Andersen[9] shows a significant difference between the self-diffusion of A and B particles. As a matter of fact, this LJ system does not show a strong avoidance of the minority species B and there is no prepeak in the partial structure factor for the BB correlations, $S_{BB}(q)$.[11] Thus, in this system the minority species B is not built into the local environment of A particles and thus the tagged particle dynamics for both species is different. In this respect, the LJ mixture reflects the entropy-driven mixing of particles of different size, as, e.g., in hard-sphere mixtures. Recent MCT calculations on Zr_2Ni,[22] where the diffusivity of both species was again found to be identical, indicate that the quantitative similarity in transport coefficients of the individual species might be a general feature for a larger class of metallic alloys.

More information about structural relaxation can be obtained from the incoherent and coherent intermediate scattering functions that we have defined in Eqs. (6) and (5), respectively. In Fig. 7, we present $F_s^{(\alpha)}(q,t)$ for both Al and Ni atoms as a function of time in the temperature range 2250 K$\geq T\geq$665 K. The results are presented for the fixed wave number q=2.7 Å^{-1}. This wave number is close to the location of the first maximum in $S_{AlAl}(q)$. At high temperatures, the function decays to zero on a picosecond time scale; here, the decay can be well fitted by an exponential function. At low temperatures, there is a two-step decay due to the cage effect. The so-called "β-relaxation" is the time regime around the plateau, while the final decay from this plateau to zero is called "α-relaxation." Note that at the lowest temperature, T=665 K, the functions $F_s^{(\alpha)}(q,t)$ decay to zero on a time scale of about 100 ns. Also the incoherent intermediate scattering functions are very similar for Al and Ni atoms, thus showing again that with respect to the tagged particle dynamics one can hardly distinguish between both species.

A two-step decay of intermediate scattering functions, as the one observed in Fig. 7, is predicted for glassforming liquids by MCT.[5,6] Moreover, MCT makes detailed predictions about the functional form of the intermediate scattering functions in the vicinity of a critical temperature T_c that marks the transition to a glassy state. An important prediction of MCT for the α relaxation regime is that close to the critical temperature the shape of time-dependent correlation functions does not depend on temperature. This property is called time-temperature superposition principle (TTSP). The TTSP means that a time-dependent correlation function $\Phi(t)$ can be written as

$$\Phi(t) = \hat{\Phi}(t/\tau(T)), \tag{15}$$

where $\tau(T)$ is the structural relaxation time (or α-relaxation time) at the temperature T. In order to define an α-relaxation time for $F_s^{(\alpha)}(q,t)$, we follow the definition that for t

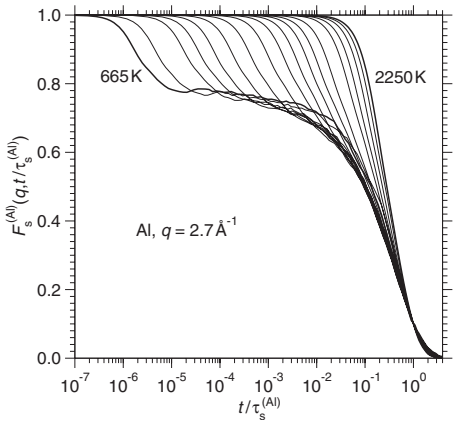

FIG. 8. Test of the time-temperature superposition principle for $F_s^{(\mathrm{Al})}(q,t)$, i.e., the data from Fig. 7(a) are plotted as a function of the scaled time $t/\tau_s^{(\mathrm{Al})}$ (with $\tau_s^{(\mathrm{Al})}$ defined by $F_s^{(\mathrm{Al})}(q,t=\tau_s^{(\mathrm{Al})})=0.1$).

$=\tau_s^{(\alpha)}(q,T)$, the scattering function has decayed to a value of 0.1, i.e., $F_s^{(\alpha)}(q,t=\tau_s^{(\alpha)}(q,T))=0.1$.

In Fig. 8, we demonstrate the validity of the TTSP for the present system. For the sake of brevity, we present results for Al only, also because the decay of the correlators for Ni is almost identical to that of Al. The curves for the different temperatures collapse nicely onto a master curve, except for the very high temperatures where the correlators do not exhibit a pronounced two-step decay.

Another prediction of MCT concerns the temperature dependence of the α-relaxation time scale: The relaxation time τ is predicted to diverge at the critical temperature,

$$\tau(T) \propto (T - T_c)^{-\gamma}, \tag{16}$$

with γ as a critical exponent which is system dependent. There is a similar prediction for the self-diffusion constants that are supposed to vanish at the critical point,

$$D_\alpha \propto (T - T_c)^{\gamma}. \tag{17}$$

Equations (16) and (17) can be checked by plotting, respectively, $\tau^{-1/\gamma}$ and $D_\alpha^{1/\gamma}$ as a function of temperature, as done in Fig. 9 for D_{Al} and $\tau_s^{(\mathrm{Al})}(q,T)$ at the wave numbers q

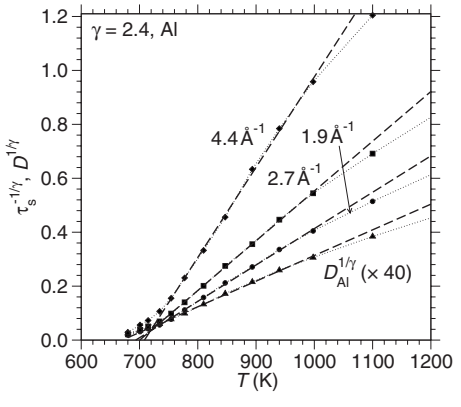

FIG. 9. Plot of $(\tau_s^{(\mathrm{Al})})^{-(1/\gamma)}$ and $D_{\mathrm{Al}}^{1/\gamma}$ as a function of temperature, using γ=2.4. The units for $\tau_s^{(\mathrm{Al})}$ and D_{Al} are ps and m^2s^{-2}, respectively. Note that $D_{\mathrm{Al}}^{1/\gamma}$ is multiplied by a factor of 40 for clarity.

$=1.9$ Å^{-1}, 2.7 Å^{-1}, and 4.4 Å^{-1}. If the MCT prediction is correct, then the data should be on a straight line, crossing the abscissa at T_c. Indeed, we find that using a value of $\gamma=2.4$, the curves show this behavior in a substantial temperature interval, as highlighted by the linear fits shown in the figure (dashed lines). The value of the exponent is in excellent agreement with the MCT calculation, solving Eq. (9), which gives $\lambda \approx 0.71$, yielding $\gamma \approx 2.35$. The linear fits intersect the T axis around 700 K, providing the simulation estimate for the critical temperature T_c of our model of $Al_{80}Ni_{20}$. The value obtained from the MCT calculations is $T_c \approx 1037$ K, some 300 K above the simulation estimate. This discrepancy is in line with previous findings.[11] It seems that the MCT approximation overestimates the freezing tendency of dense liquids in general.

Deviations from the power-law predictions [Eqs. (16) and (17)] can be inferred in Fig. 9 on the one hand for high temperatures, $T>1000$ K. This can be expected because the asymptotic MCT predictions, Eqs. (16) and (17), require the vicinity of the critical point and thus do not hold if the temperatures are too high. On the other hand, deviations from the predicted power law are seen at low temperatures, say for $T<720$ K. This is due to the fact that a divergence at T_c, as predicted by MCT, is not found in reality. Once the relaxation times have increased beyond a value of about 10 ns for atomistic systems such as $Al_{80}Ni_{20}$, the system starts to relax via relaxation channels that can be taken into account by the theory only by "*ad hoc*" schematic models.[5,6,46,47] These relaxation channels, often called hopping processes, lead to finite relaxation times at and below the critical temperature. However, versions of MCT, which include hopping processes in the aforementioned *ad hoc* manner, yield the interesting result that some predictions for the β-relaxation regime are unaffected by the hopping processes.[48] Below, we discuss these predictions for the Al-Ni alloy considered in this work.

A closer inspection of Fig. 9 reveals that one would obtain a significantly lower T_c from the self-diffusion constant, D_{Al}, than from the relaxation times at the different wave numbers. This decoupling of the self-diffusion constant from the relaxation times has also been found in computer simulations of other glassforming liquids, such as hard-sphere mixtures,[49] the binary Lennard-Jones mixture[8] and glassformers with a tetrahedral network structure such as water,[50] silica,[51] and germania.[52] In order to quantify the decoupling between the α relaxation time scale and self-diffusion, we plot in Fig. 10 the product of D_{Al} with the relaxation time $\tau_s^{(\mathrm{Al})}(q,T)$ for different values of q. According to MCT, the product $\tau_s^{(\mathrm{Al})} \times D_{\mathrm{Al}}$ should be a constant in the vicinity of T_c. Indeed, this product is almost constant at high temperatures, but it increases significantly below about 900 K. The inset of Fig. 10 shows the same data, multiplied by a constant factor, such that the product $\tau_s^{(\mathrm{Al})} \times D_{\mathrm{Al}}$ approaches about 1 Å^2 at high temperatures. One sees that around the critical temperature the products of relaxation times with self-diffusion constants are about a factor of 4 to 5 higher than at high temperatures, and they are further increasing below T_c.

Recently, the relation between self-diffusion constants D_α and the shear viscosity η has been extensively discussed for glassforming liquids.[7,53] The basis for this discussion is the

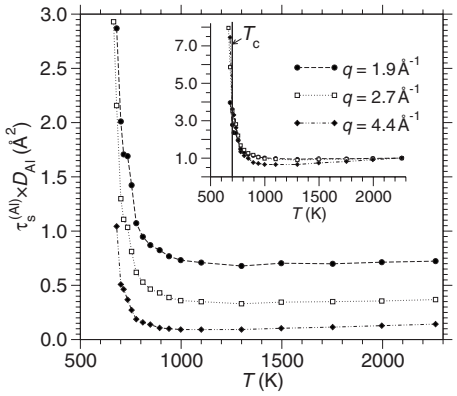

FIG. 10. Plot of the product $\tau_s^{(\mathrm{Al})} \times D_{\mathrm{Al}}$ for three different values of wave number q, as indicated. The inset shows the same data, but now multiplied by constant factors, such that the product $\tau_s^{(\mathrm{Al})} \times D_{\mathrm{Al}}$ approaches 1 Å^2 at high temperatures. The vertical line in the inset marks the location of critical mode coupling temperature, $T_c \approx 700$ K.

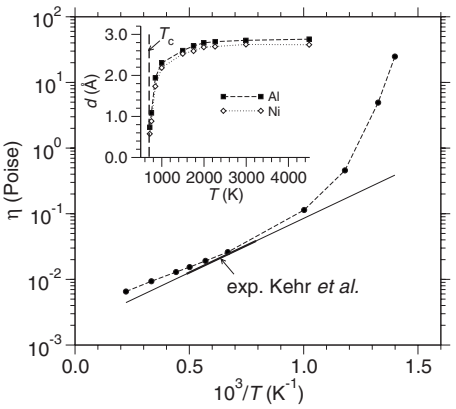

FIG. 11. Shear viscosity η as a function of inverse temperature. Also included are experimental data by Kehr *et al.* (Ref. 55) (the bold part of the dashed-dotted Arrhenius line, as extracted from the experiment, corresponds to the temperature range where the measurements were performed). The inset shows the Stokes-Einstein-Sutherland diameter d_α for both Ni and Al atoms as a function of temperature. d_α was calculated from Stokes-Einstein-Sutherland relation (18).

so-called Stokes-Einstein-Sutherland relation,[27]

$$D_\alpha = \frac{k_B T}{c \pi \eta d_\alpha}, \tag{18}$$

which can be derived for a big (macroscopic) sphere of diameter d_α that moves through a viscous medium with a shear viscosity η. In Eq. (18), k_B is the Boltzmann constant. The constant c depends upon the specific boundary condition on the surface of the sphere. For slip boundary conditions $c=2$ and for no-slip boundary conditions $c=3$.[27]

Surprisingly, Eq. (18) is often also found to hold for a tagged particle in a dense liquid with viscosity η, where the tagged particle is identical to its surrounding particles. For the "normal liquid state," this can be explained by the fact that hydrodynamics seems to hold down to the molecular scale, provided that properties in the long-time limit (or zero-frequency limit) are considered. This has been demonstrated in a recent study by Horbach and Succi[54] and is not at all trivial since the hydrodynamic limit is expected to be only valid for long times *and* macroscopic length scales.

There is even evidence from different experimental studies that the Stokes-Einstein-Sutherland relation is also valid for glassforming liquids just above the mode-coupling temperature T_c, in particular for massive metallic glassformers.[28–30] In order to check the Stokes-Einstein-Sutherland relation for the model of $Al_{80}Ni_{20}$ considered in this work, we have computed the shear viscosity from the Green-Kubo relation[39]

$$\eta(T) = \frac{1}{k_B T V} \int_0^\infty dt \langle \sigma_{\alpha\beta}(0) \sigma_{\alpha\beta}(t) \rangle, \quad \alpha \neq \beta, \tag{19}$$

where the off-diagonal elements of the pressure tensor (i.e., those with $\alpha \neq \beta$) are given by

$$\sigma_{\alpha\beta}(t) = \sum_{k=1}^{N} \left[m_k v_k^\alpha v_k^\beta + \frac{1}{2} \sum_{l(\neq k)} F_{kl}^\alpha r_{kl}^\beta \right], \tag{20}$$

with v_k^α, F_{kl}^α, and r_{kl}^α as the α component of the velocity of particle k, the force between particles k and l, and the distance between particles k and l, respectively.

In Fig. 11, the logarithm of the shear viscosity is plotted as a function of inverse temperature. Also included are recent experimental data by Kehr *et al.*[55] The simulation is in excellent agreement with the experiment. Note that in Ref. 55, an Arrhenius law was fitted to the data; this is shown as a dashed-dotted line in the figure. Obviously, the simulation reveals that, similar to the α relaxation times and the self-diffusion constants, the increase of η with decreasing temperature is highly non-Arrhenius. The inset of Fig. 11 shows the Stokes-Einstein-Sutherland diameter as a function of temperature, as calculated from the simulation data for η and D_α via Eq. (18). For the constant c in Eq. (18), we have used $c=2$, assuming slip boundary conditions at the "surface" of the atoms. At high temperature, the Stokes-Einstein-Sutherland diameter is in fact approximately constant, yielding a value around 2.8 Å both for Al and Ni atoms. This value corresponds approximately to the location of the first maximum in $g_{\mathrm{AlAl}}(r)$. Below about 1800 K, the diameter d_α starts to decrease, reaching a value of about 0.5 Å at the critical MCT temperature T_c. Thus, the Stokes-Einstein-Sutherland diameter is about a factor of 5 smaller at T_c than at temperatures above, say 2000 K. Note that a similar finding has been obtained for the binary Lennard-Jones mixture.[32]

A comparison between Fig. 10 and Fig. 11 reveals that the "decoupling" of the self-diffusion constants from the α-relaxation times seems to be less pronounced than the decoupling of self-diffusion and viscosity. At T_c, it is about a factor of 3 for the former case and a factor of 5 for the latter

case. But this has probably a rather trivial reason. It can be explained by the variation due to the factor k_BT in SES relation (18) which leads to a decrease in the SES diameter d_α with decreasing temperature. As mentioned before there is no reason why SES relation (18) should hold in the undercooled regime. In the framework of MCT, the self-diffusion constant and the shear viscosity are predicted to follow power laws of forms (17) and (16), respectively. These power laws are supposed to hold as T approaches T_c from above, so that the product $D_\alpha\eta$ approaches a finite value and does not diverge. Farther away from T_c, corrections to scaling usually lead to minor violations of the SES relation, that are however much smaller than what is observed in simulation.

In addition to the predictions for the α-relaxation regime, MCT makes also detailed predictions for the β-relaxation regime. For the late β-relaxation regime (or the short-time regime of the α-relaxation), the following formula for the time correlator (being either the incoherent or coherent intermediate scattering function) is found:[56]

$$\Phi(q,t) = f^c(q) - h_c(q)t^b + h_2(q)t^{2b} + \ldots . \qquad (21)$$

Here, $h_c(q)$ is the so-called critical amplitude that depends, as the amplitude $h_2(q)$, on the wave number q. $f^c(q)$ is the height of the plateau in the intermediate scattering function, corresponding to the Lamb-Mößbauer (LM) and the DW factors of the incoherent and coherent intermediate scattering functions, respectively. $f^c(q)$ is also known as the nonergodicity parameter. This function expresses the "decorrelation" of the system from its state at time $t=0$ due to the rattling motion of the particles in their cage.

The first two terms of Eq. (21) form the so-called von Schweidler law (with b as the von Schweidler exponent). MCT predicts that b should be the same for all correlators. Moreover, there is a one-to-one correspondence with the exponent γ via the relations

$$\gamma = \frac{1}{2a} + \frac{1}{2b}, \quad \lambda = \frac{\Gamma^2(1+b)}{\Gamma(1+2b)} = \frac{\Gamma^2(1-a)}{\Gamma(1-2a)}, \qquad (22)$$

with λ as the so-called exponent parameter, $\Gamma(x)$ the Gamma-function and a another critical exponent. In the analysis of the α relaxation times and self-diffusion constants we have found $\gamma=2.4$. This value of γ corresponds to $b=0.54$, using Eq. (22). The value of the exponent parameters that corresponds to these values of γ and b is $\lambda \approx 0.76$.

In Fig. 12, the dashed curves correspond to fits with Eq. (22) to $F_s^{(\mathrm{Al})}(q,t)$ as well as to the coherent intermediate scattering functions $F^{(\mathrm{AlAl})}(q,t)$ and $F^{(\mathrm{NiNi})}(q,t)$ at different values of q. The temperature is $T=680$ K. In the fitting process, the exponent b was kept fixed at 0.54. The quality of the fits suggests that the prediction [Eq. (21)] is well valid for our system.

From the fits to the intermediate scattering functions with Eq. (21), we have determined the q dependence of DW and LM factors, $f^{(\alpha\alpha)}(q)$ and $f_s^{(\alpha)}$, respectively. The different DW and LM factors are shown in Fig. 13 for $T=680$ K. The LM factors almost coincide for Al and Ni atoms, thus indicating again that the one-particle dynamics is almost identical for

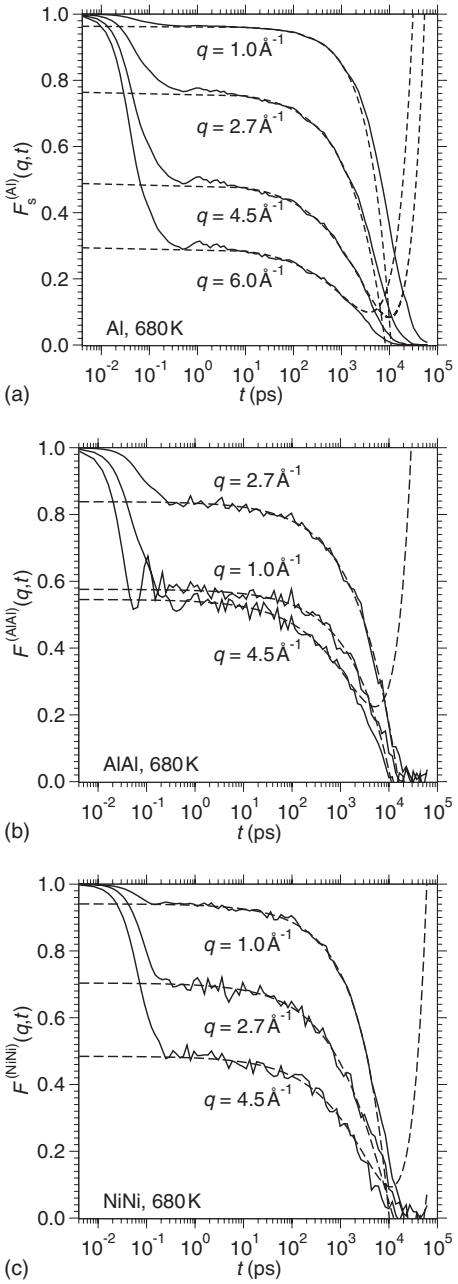

FIG. 12. Incoherent intermediate scattering function $F_s^{(\mathrm{Al})}(q,t)$ (a) as well as coherent intermediate scattering functions $F^{(\mathrm{AlAl})}(q,t)$ (b) and $F^{(\mathrm{NiNi})}(q,t)$ (c) for the indicated wave numbers at $T=680$ K. The dashed lines are fits to the MCT prediction [Eq. (21)], using $b=0.54$ for the von Schweidler exponent.

Al and Ni atoms. The monotonous decay of the LM factors to zero can be well described by a Gaussian of the form $f_s^{(\alpha)}(q)=\exp[-(1/6)\langle r^2_{\mathrm{plat},\alpha}\rangle q^2]$ where $\langle r^2_{\mathrm{plat},\alpha}\rangle$ corresponds to the height of the plateau in the mean-squared displacement $\langle r_\alpha^2(t)\rangle$. In fact, fits with the latter Gaussian yield $\langle r^2_{\mathrm{plat,Al}}\rangle = \langle r^2_{\mathrm{plat,Ni}}\rangle \simeq 0.198$. This value is indeed the height of the plateau in the mean-squared displacements at $T=680$ K (see Fig. 6).

The DW factors oscillate around the LM factors. These oscillations reflect features also seen in the partial static structure factors. In a one-component system, $S(q)$ and $f(q)$

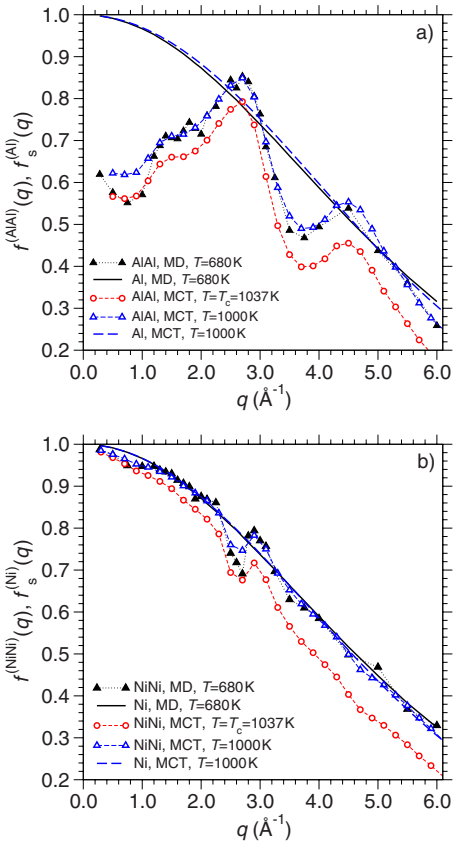

FIG. 13. (Color online) Lamb-Mößbauer factors as well as Debye-Waller factors for aluminum (a) and nickel (b), at $T=680$ K as a function of wave number. Also shown are results from a MCT calculation using the partial structure factors from the simulation as input (for details see text).

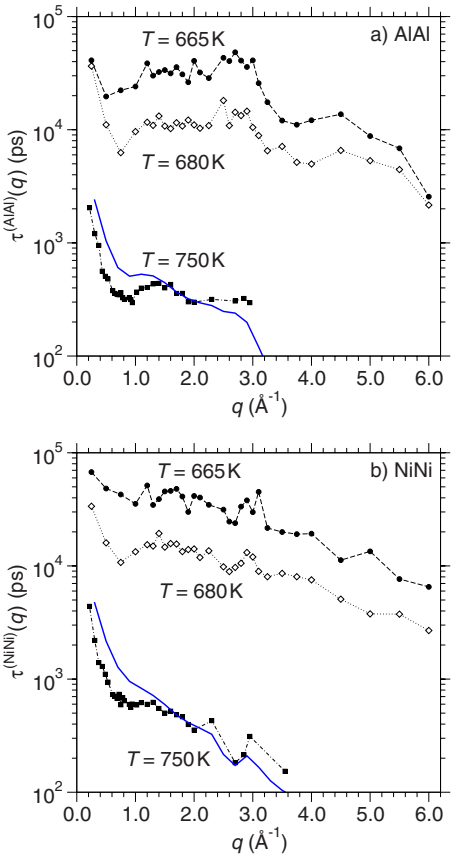

FIG. 14. (Color online) q dependence of coherent relaxation times $\tau^{(\mathrm{AlAl})}(q)$ (a) and $\tau^{(\mathrm{NiNi})}(q)$ for three different temperatures, as indicated. The solid lines are results from MCT at $T=1050$ K, scaled by a factor 10^{-3}.

are seen to vary strongly in phase as functions of q, while for mixtures, this strict relation is not necessarily true. Indeed, the function $f^{(\mathrm{AlAl})}(q)$ displays two peaks at $q=2.8$ Å^{-1} and at $q=4.7$ Å^{-1} that correspond to the locations of the first two peaks in the partial static structure factor $S_{\mathrm{AlAl}}(q)$ (see Fig. 4). But $f^{(\mathrm{AlAl})}(q)$ shows also a broad shoulder in the range 1.4 Å$^{-1}\leq q\leq 2.0$ Å^{-1}, i.e., in the region where a prepeak appears in $S_{\mathrm{NiNi}}(q)$. This is very remarkable because the latter prepeak is not seen in $S_{\mathrm{AlAl}}(q)$. Thus, the simple notion that the oscillations in the DW factors $f^{(\alpha\alpha)}(q)$ are in phase with the oscillation in the corresponding partial structure factors $S_{\alpha\alpha}(q)$ is not true for our system.

As can be also inferred from Fig. 13, the oscillations in $f^{(\mathrm{AlAl})}(q)$ are much more pronounced than in $f^{(\mathrm{NiNi})}(q)$, with the latter function being close to the LM factors. These differences are due to the relatively strong asymmetry of the concentration in the 80:20 mixture considered in this work. At small q, collective vibrational excitations (sound modes) are naturally more strongly revealed in the collective correlations of the majority species Al. Therefore, the function $f^{(\mathrm{AlAl})}(q)$ drops to a relatively small value of about 0.6 at small q, whereas $f^{(\mathrm{NiNi})}(q)$ is close to one here. For larger q, structural features are reflected in a more pronounced manner in the majority species, thus yielding the strong oscillations in $f^{(\mathrm{AlAl})}(q)$.

Also shown in Fig. 13 are the results from the MCT calculations for the DW and LM factors at the temperatures $T=T_c\approx 1037$ K and $T=1000$ K, the former being the prediction of the critical temperature T_c from the theory. The MCT results for the $f^{(\alpha\alpha)}(q)$ agree qualitatively with the values obtained from the simulations. In particular, all oscillations discernible in our data are reproduced. However, the values of the DW factors at $T=T_c$ are systematically below the simulation results. Partially, this is related to the overestimation of the freezing tendency in the theory, predicting dynamical arrest already at higher temperatures where the localization of the particles is less pronounced, and also known from the binary LJ system.[11] Note also that the fits to the simulation data were done at $T=680$ K, slightly below the estimated T_c, and that for $T<T_c$, both the DW and LM factors rise continuously with lowering T. The MCT-calculated values for $T=1000$ K, some 40 K below T_c, in fact agree nicely with the simulation results, as shown in the figure.

The striking emergence of a shoulder in the AlAl-DW factors on length scales corresponding to the NiNi prepeak in the equilibrium static structure is also reproduced by MCT. There, it arises quite naturally because the memory kernel appearing in Eq. (9) mixes contributions from all partial density fluctuations. The fact that such Ni-Ni correlations transcend to the Al-Al dynamics nicely illustrates the difference between equilibrium properties of the melt (as exhibited by

the static structure factor) and the structure attained in the glassy state (as described by the DW factor).

The relationship between structural features and structural relaxation can be also investigated by means of the q dependence of the α relaxation times for the coherent intermediate scattering functions. In Fig. 14, the α relaxation times $\tau^{(\mathrm{AlAl})}(q)$ and $\tau^{(\mathrm{NiNi})}(q)$ are displayed for three different temperatures. Obviously, the functional form of the relaxation times is very similar for the Al-Al and the Ni-Ni correlations. It does not change also qualitatively with temperature. In $\tau^{(\mathrm{AlAl})}(q)$, we see a broad shoulder around a wave number of $q=1.8$ Å^{-1}, corresponding to location of the prepeak in $S_{\mathrm{NiNi}}(q)$. So we observe again this feature in the Al-Al correlations and thus, also $\tau^{(\mathrm{AlAl})}(q)$ is not in phase with the corresponding static structure factor $S_{\mathrm{AlAl}}(q)$.

As the solid lines in Fig. 14 show, this coupling of the relaxation times is also captured by MCT. In this calculation, we have obtained $\tau_{\alpha\beta}(q)$ from the solutions to the dynamical MCT equations, Eq. (7), at $T=1050$ K, slightly above T_c, and using the same definition for the relaxation times as in the MD simulation. The relaxation times obtained in this way are unreasonably high due to the vicinity of the MCT divergence. In order to allow a meaningful comparison, we have arbitrarily divided the MCT values for $\tau_{\alpha\beta}(q)$ by a constant factor of 1000. After this rescaling, they demonstrate that the theory describes reasonably well the spatial dependence of the relaxation of the different types of density fluctuations in the system.

IV. SUMMARY AND DISCUSSION

In this paper, results from extensive MD simulations of undercooled $Al_{80}Ni_{20}$ at constant pressure ($p=0$) have been presented. We have focused on the relation between chemical ordering and structural relaxation. After having discussed the behavior of partial pair correlation functions and partial static structure factors, intermediate scattering functions have been analyzed in the framework of MCT. Also the relation between one-particle and collective dynamics has been studied, in particular checking the validity of the SES relation between self-diffusion and shear viscosity.

The structure of $Al_{80}Ni_{20}$ is similar to that of densely packed system of hard spheres. However, the chemical ordering in the Al-Ni system is different from that found in hard spheres. The Ni atoms tend to avoid other Ni atoms as nearest neighbors and this leads to the presence of CSRO, i.e., in this case, to an inhomogeneous distribution of Ni atoms on intermediate length scales. As a consequence, the partial static structure factor for the Ni-Ni correlations, $S_{\mathrm{NiNi}}(q)$, exhibits a broad prepeak around $q=1.8$ Å^{-1}. Such a feature is absent in the binary 80:20 LJ mixture that has been put forward by Kob and Andersen.[8]

The CSRO has interesting effects on structural relaxation and transport properties. The one-particle dynamics of Al and Ni atoms is very similar, as we have shown with respect to the mean-squared displacements and the incoherent intermediate scattering functions. Therefore, the self-diffusion constants and the incoherent α relaxation times are almost the same for Al and Ni atoms. The same holds for the Lamb-Mößbauer factors which indicates that Al atoms are as localized as Ni atoms, albeit the atomic radius of the two species is different. The similarity in the structural relaxation of the two species is also seen in the collective dynamics. The differences in the DW factors for the Al-Al and Ni-Ni correlations can be referred to the fact that the considered mixture has a large asymmetry with respect to the concentrations of Al and Ni atoms. But the prepeak in $S_{\mathrm{NiNi}}(q)$ is also reflected in the DW factor and α relaxation time for the Al-Al correlations. Thus, the latter features are not in phase with the partial structure factor for the Al-Al correlations, $S_{\mathrm{AlAl}}(q)$, contradicting the common folklore.

In this paper, we have studied the dynamics of fully equilibrated melts on time scales up to 100 ns. The lowest considered temperature, $T=665$ K, is slightly below the critical MCT temperature which is approximately at 700 K for our system. The relaxation dynamics of $Al_{80}Ni_{20}$, as seen by the simulation, is compatible with the predictions of MCT. However, as in several other glassforming systems,[7] the self-diffusion constants show a significantly different temperature dependence than the α relaxation times and the shear viscosity. This is in disagreement with MCT. Recently, Biroli and Bouchaud[53] have proposed some ideas to reconcile the "breakdown of the SES relation" in the framework of MCT.[53] They have argued that critical dynamical fluctuations have to be taken into account in order to describe the failure of SES. The standard version of the theory is a kind of mean-field theory and thus, such fluctuations are neglected. It has to be seen whether the explanation proposed by Biroli and Bouchaud is the correct one.

By applying MCT to the equilibrium static structure factors obtained from simulation, we could show that the theory is able to capture the subtle interplay between the different length scales set by the Ni-Ni and Al-Al interactions. In particular, the effect that structural correlations appearing only for the Ni atoms in the equilibrium structure also emerge for the dynamical Al-Al correlations is quite naturally explained by the multicomponent MCT equations. While the generic features found in MCT do not differ qualitatively from those found for simple hard-sphere mixtures,[41,57] our study complements a recent application of MCT to experimental structure factors on Zr_2Ni (Ref. 22) in showing that the theory can describe a number of dynamical consequences arising from strong chemical short-range ordering.

ACKNOWLEDGMENTS

Useful discussions with K. Binder and A. Meyer are gratefully acknowledged. We are grateful for financial support within the Priority Programme 1120 *Phase Transformations in Multicomponent Melts* of the Deutsche Forschungsgemeinschaft. T.V. thanks the Helmholtz-Gemeinschaft for funding through the Impuls-und Vernetzungsfonds research group under Grant No. VH-NG 406. S.K.D. is grateful to K. Binder and J.H. for supporting his stay in Mainz where all the simulations were performed. A generous grant of computing time at the NIC Jülich is gratefully acknowledged.

[1] N. E. Cusack, *The Physics of Structurally Disordered Matter: An Introduction* (IOP, Bristol, 1987).
[2] D. Mayou and A. Pasturel, J. Phys.: Condens. Matter **1**, 9685 (1989).
[3] M. Maret, T. Pomme, A. Pasturel, and P. Chieux, Phys. Rev. B **42**, 1598 (1990).
[4] S. K. Das, J. Horbach, M. M. Koza, S. Mavila Chatoth, and A. Meyer, Appl. Phys. Lett. **86**, 011918 (2005).
[5] W. Götze and L. Sjögren, Rep. Prog. Phys. **55**, 241 (1992).
[6] W. Götze, J. Phys.: Condens. Matter **11**, A1 (1999).
[7] K. Binder and W. Kob, *Glassy Materials and Disordered Solids: An Introduction to Their Statistical Mechanics* (World Scientific, London, 2005).
[8] W. Kob and H. C. Andersen, Phys. Rev. Lett. **73**, 1376 (1994).
[9] W. Kob and H. C. Andersen, Phys. Rev. E **51**, 4626 (1995).
[10] W. Kob and H. C. Andersen, Phys. Rev. E **52**, 4134 (1995).
[11] M. Nauroth and W. Kob, Phys. Rev. E **55**, 657 (1997).
[12] T. Gleim, W. Kob, and K. Binder, Phys. Rev. Lett. **81**, 4404 (1998).
[13] T. Gleim and W. Kob, Eur. Phys. J. B **13**, 83 (2000).
[14] W. Kob, *Supercooled Liquids, the Glass Transition, and Computer Simulations*, Lecture Notes for Les Houches Sesssion LXXVII: Slow Relaxations and Nonequilibrium Dynamics in Condensed Matter, Les Houches, 1–25 July 2002, edited by J.-L. Barrat, M. Feigelman, J. Kurchan, and J. Dalibard (Springer, Berlin, 2003), pp. 199–270.
[15] H. R. Schober, Phys. Rev. Lett. **88**, 145901 (2002).
[16] M. Kluge and H. R. Schober, Phys. Rev. B **70**, 224209 (2004).
[17] H. R. Schober, Phys. Chem. Chem. Phys. **6**, 3654 (2004).
[18] H. Teichler, Phys. Rev. Lett. **76**, 62 (1996).
[19] A. B. Mutiara and H. Teichler, Phys. Rev. E **64**, 046133 (2001).
[20] X. J. Han and H. Teichler, Phys. Rev. E **75**, 061501 (2007).
[21] F. Faupel, W. Frank, M.-P. Macht, H. Mehrer, V. Naundorf, K. Rätzke, H. R. Schober, S. K. Sharma, and H. Teichler, Rev. Mod. Phys. **75**, 237 (2003).
[22] Th. Voigtmann, A. Meyer, D. Holland-Moritz, S. Stüber, T. Hansen, and T. Unruh, Europhys. Lett. **82**, 66001 (2008).
[23] J. Horbach, S. K. Das, A. Griesche, M.-P. Macht, G. Frohberg, and A. Meyer, Phys. Rev. B **75**, 174304 (2007).
[24] L. S. Darken, Trans. AIME **180**, 430 (1949).
[25] A. Kerrache, J. Horbach, and K. Binder, Europhys. Lett. **81**, 58001 (2008).
[26] W. Sutherland, Philos. Mag. **9**, 781 (1905); The independent contribution of Sutherland is being acknowledged only recently: For references, see S. K. Das, J. V. Sengers, and M. E. Fisher, J. Chem. Phys. **127**, 144506 (2007); T. M. Squires and J. F. Brady, Phys. Fluids **17**, 073101 (2005).
[27] L. D. Landau and E. M. Lifshitz, *Fluid Mechanics* (Pergamon, New York, 1987).
[28] A. Meyer, Phys. Rev. B **66**, 134205 (2002).
[29] V. Zöllmer, K. Rätzke, F. Faupel, and A. Meyer, Phys. Rev. Lett. **90**, 195502 (2003).
[30] A. Bartsch, K. Rätzke, F. Faupel, and A. Meyer, Appl. Phys. Lett. **89**, 121917 (2006).
[31] A. Meyer, W. Petry, M. M. Koza, and M. P. Macht, Appl. Phys. Lett. **83**, 3894 (2003).
[32] P. Bordat, F. Affouard, M. Descamps, and F. Müller-Plathe, J. Phys.: Condens. Matter **15**, 5397 (2003).
[33] A. M. Puertas, C. De Michele, F. Sciortino, P. Tartaglia, and E. Zaccarelli, J. Chem. Phys. **127**, 144906 (2007).
[34] J. Horbach and W. Kob, Phys. Rev. B **60**, 3169 (1999).
[35] Y. Mishin, M. J. Mehl, and D. A. Papaconstantopoulos, Phys. Rev. B **65**, 224114 (2002).
[36] D. Frenkel and B. Smit, *Understanding Molecular Simulation: From Algorithms to Applications* (Academic, San Diego, 1996).
[37] T. B. Massalski, *Binary Alloys Phase Diagrams* (ASM, Metals Park, OH, 1990).
[38] Y. Plevachuk, I. Egry, J. Brillo, D. Holland-Moritz, and I. Kaban, Int. J. Mater. Res. **98**, 107 (2007).
[39] M. P. Allen and D. J. Tildesley, *Computer Simulation of Liquids* (Clarendon, Oxford, 1987).
[40] J.-P. Hansen and I. R. McDonald, *Theory of Simple Liquids*, 3rd ed. (Academic, London, 2006).
[41] W. Götze and Th. Voigtmann, Phys. Rev. E **67**, 021502 (2003).
[42] L. L. Lee, J. Phys. Chem. **60**, 1197 (1974).
[43] F. Sciortino and W. Kob, Phys. Rev. Lett. **86**, 648 (2001).
[44] T. Schenk, D. Holland-Moritz, V. Simonet, R. Bellissent, and D. M. Herlach, Phys. Rev. Lett. **89**, 075507 (2002).
[45] A. B. Bhatia and D. E. Thornton, Phys. Rev. B **2**, 3004 (1970).
[46] S. P. Das and G. F. Mazenko, Phys. Rev. A **34**, 2265 (1986).
[47] W. Götze and L. Sjögren, Z. Phys. B: Condens. Matter **65**, 415 (1987).
[48] M. Fuchs, W. Götze, S. Hildebrand, and A. Latz, J. Phys.: Condens. Matter **4**, 7709 (1992).
[49] G. Foffi, W. Götze, F. Sciortino, P. Tartaglia, and Th. Voigtmann, Phys. Rev. E **69**, 011505 (2004).
[50] F. W. Starr, F. Sciortino, and H. E. Stanley, Phys. Rev. E **60**, 6757 (1999).
[51] J. Horbach and W. Kob, Phys. Rev. E **64**, 041503 (2001).
[52] M. Hawlitzky, J. Horbach, S. Ispas, M. Krack, and K. Binder, J. Phys.: Condens. Matter **20**, 285106 (2008).
[53] G. Biroli and J. P. Bouchaud, J. Phys.: Condens. Matter **19**, 205101 (2007).
[54] J. Horbach and S. Succi, Phys. Rev. Lett. **96**, 224503 (2006).
[55] M. Kehr, M. Schick, I. Egry, and W. Hoyer, High Temp. High Press (to be published).
[56] T. Franosch, W. Götze, M. R. Mayr, and A. P. Singh, Phys. Rev. E **55**, 3183 (1997).
[57] Th. Voigtmann, Phys. Rev. E **68**, 051401 (2003).